Dalton Transactions

An international journal of inorganic chemistry

Accepted Manuscript

This article can be cited before page numbers have been issued, to do this please use: J. Langwald, S. Burguera Piña, A. Frontera and M. S. Wickleder, *Dalton Trans.*, 2026, DOI: 10.1039/D6DT01140C.

ROYAL SOCIETY OF CHEMISTRY

rsc.li/dalton

View Article Online
DOI: 10.1039/D0DT01140C

Chalcogen Bonding vs. Weakly Coordinating Anions – A Solid State Study on Halidoselenium Cations in an Oxoanionic Environment.

Jan Langwald,[a] Sergi Burguera,[b] Antonio Frontera *[b] and Mathias S. Wickleder*[a]

[a] *Institute of Inorganic and Materials Chemistry, University of Cologne, Greinstr. 6, 50939 Cologne, Germany. E-mail: mathias.wickleder@uni-koeln.de*

[b] *Universitat de les Illes Balears, Crta de Valldemossa km 7.5, 07122 Palma de Mallorca, Baleares, Spain. E-mail: toni.frontera@uib.es*

Abstract

We present the crystal structure of selenoyl chloride, $SeOCl_2$, for the first time and show that it can be used for the subsequent synthesis of novel compounds with the $[SeCl_3]^+$ cation, which we stabilized as disulfate $[S_2O_7]^{2-}$ and chlorosulfate $[ClSO_3]^-$ salts, respectively. Both, $SeOCl_2$ as well as the $[SeCl_3]^+$ salts show remarkable macromolecular arrangements and packing motifs in the solid state, so far not or only scarcely analyzed. Additionally, we report the stabilization of the dication $[Se_2I_4]^{2+}$ in the tetrasulfate salt $[Se_2I_4]_2[S_4O_{13}]_2(SO_3)$. This marks the very first examples of the respective cations in an oxoanionic environment. All compounds show strong and directional non-covalent interactions, i.e. chalcogen bonding, as well as, to a lesser degree, halogen bonding (HaB). These interactions were investigated via Density functional theory (DFT) investigations, i.e. molecular electrostatic potential (MEP) surface plots, quantum theory of atoms in molecules (QTAIM) and natural bond orbital (NBO) analyses. Overall, this work demonstrates that, while Coulombic forces are the primary drivers in these ionic systems, the directionality and specific orbital contributions of σ- and π-hole interactions are essential for fine-tuning the final supramolecular assemblies.

Introduction

The chemistry of the mixed group 16/17 compounds ChX_4 (Ch = Se, Te; X = Cl) and their derived cations is a textbook example for the peculiar divergence between growing discovery of new compounds within a group and their lacking correct structural elucidation. The phase pure preparation of these compounds is known since the early 20th century,[1-3] their unit cells and space groups were determined 1964,[4] but the solid state structure of the stable $SeCl_4$ modifications was only reported in 1981.[5-6] Even before the first structural reports on $SeCl_4$, *Kolditz* and *Schäfer* reported different synthetic routes towards $[ChCl_3][AsF_6]$ (Ch = S, Se, Te) via direct synthesis of the di- and tetrachlorides with AsF_3 (for sulfur) as well as chlorination of $SeCl_3$ and elemental Te.[7] Building up on the work of *Gerding*,[8] *Robinson* and *Ciruna* showed the existence of $[ChCl_3][XSO_3]$ (Ch = Se, Te; X = F, Cl) in solutions of the respective $ChCl_4$ species in XSO_3H via conductimetric and (*Raman*) spectroscopic measurements.[9] Although this work and the subsequent report by *Gerding* for the '$Ch_4{\cdot}SO_3$' adducts are long known,[10] no crystal structures of the respective chloro- or polysulfates were reported until today. This is especially puzzling, since a number of $[ChCl_3][XSO_3]$ (Ch = Se, Te; X = F_3C, CH_3, *p*-$CH_3C_6H_4$) salts was reported by *Kapoor* et al. in 1989.[11]

It was not until 1985, when *Gillespie* and *Sawyer* reported the first crystal structures of the $[ChCl_3]^+$ cations as $[SbCl_6]^-$, $[AlCl_4]^-$, $[PnF_6]^-$ (Pn = As, Sb) salts, besides $[TeF_3]_2[SO_4]$.[12] They used the common method of direct halide abstraction from $[PnX_5]$ (Pn = As, Sb; X = F,

View Article Online
DOI: 10.1039/D6DT01140C

Cl). Following this synthetic approach, subsequent reports for $[SeBr_3][GaBr_4]$,[13] $[SeCl_3][MCl_6]$ (M = Zr, Hf, Mo, Re)[14] and *β*-$[SeCl_3][MoOCl_4]$[15] were published, alongside improved synthetic procedures towards the $[PnF_6]^-$ species,[16] computational and ^{77}Se NMR studies,[17] and even the use of $[SeCl_3][AlCl_4]$ as a precursor towards the generation of $([SeP][AlCl_4])_n$.[18] Recently, the compounds $[(Se,Te)Cl_3][GaCl_4]$ gained renewed interest due to potential use as nonlinear optics materials based on their observed second harmonic generation effect, due to the stereochemically active lone-pair at the Se(IV) centre.[19]

In the context of our own research on (inter-)halogen polysulfates[20] and (poly-)chalcogen polysulfates[21], we were interested in the stabilization of mixed halidochalcogenium cations with oxoanions and the respective differences towards the classical halidometalates. Especially with regard to non-covalent interactions, namely halogen bonding (HaB)[22] and chalcogen bonding (ChB),[23] the detailed analysis of the occurring cation-anion interactions is of importance. Not only have these interactions been used for catalysis[24] and as sensors,[25] they have also been studied concerning the influence of stabilization due to co-crystal formation[26] or aggregate formation, where they can even challenge hydrogen bonds.[27]

Within our investigations, we realized that the long-known selenoyl chloride ($SeOCl_2$) was still lacking a solid-state structural characterization, since the only reported structure is the bis-pyridine adduct $[SeOCl_2]\cdot[C_5H_5N]_2$.[28] Thus, we first prepared $SeOCl_2$ from SeO_2, $SOCl_2$ and Cl_2 as reported in the literature,[29] crystallized the compound at 7°C and investigated its solid-state structure. Subsequently, we used the $SeOCl_2$ for the preparation of $[SeCl_3]_2[S_2O_7]$ (**1**) and $[SeCl_3][ClSO_3]$ (**2**), which are obtained depending on the applied reaction temperatures (see Figure 1).

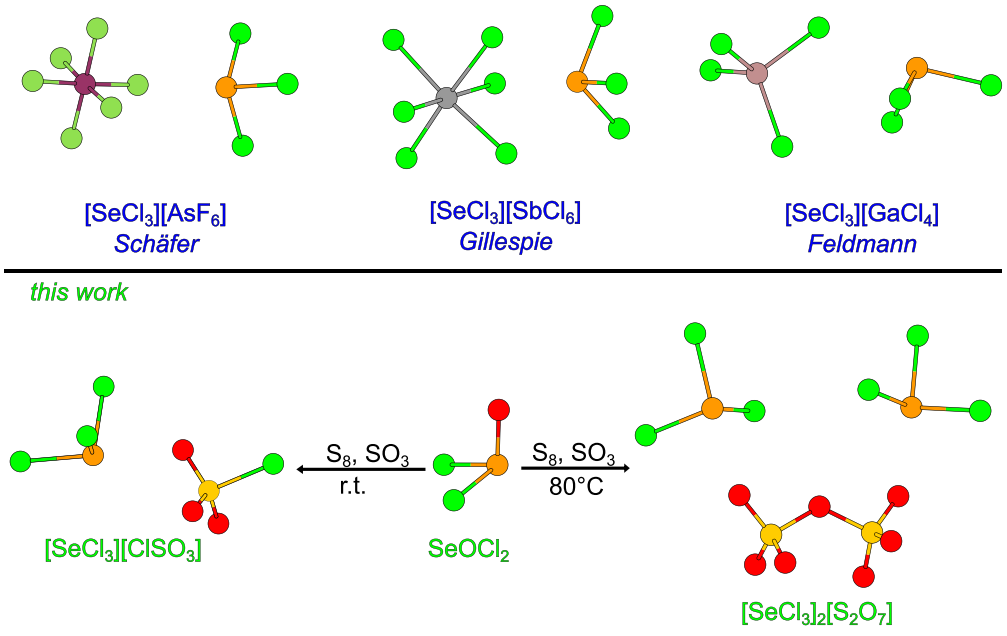

Figure 1: Literature-known $[SeCl_3]^+$ compounds and two of the novel compounds presented herein. The shown structures represent the simplest building blocks of the respective solid-state structures.

Furthermore, we aimed for the isolation of the respective heavier homologues $[SeBr_3]^+$ and $[SeI_3]^+$. However, we were only able to isolate $[Se_2I_4]_2[S_4O_{13}]_2\cdot(SO_3)$ (**3**) from direct solvothermal reaction of the elements with neat SO_3. Lastly, we performed an in-depth quantum

View Article Online
DOI: 10.1039/D6DT01140C

chemical analysis of the electrostatic potentials and the non-covalent interactions within all novel compounds, which can be directly related to the observed bond lengths and donor-acceptor distances within the solid-state structures.

Results and Discussion

The starting material for our investigations, $SeOCl_2$, is a colorless to pale-yellow liquid at room temperature, which crystallizes upon cooling below ~10 °C. We were able to measure its crystal structure using an in-house-made apparatus for the handling of crystals at lower temperatures, based on the *Stalke* apparatus.[30] The compound crystallizes in the centrosymmetric space group $P2_1/n$ (No. 14) with 24 formula units per unit cell (see ESI, p. 3–8). The unusually large unit cell, especially in case of a simple molecular compound, differs significantly from that of the lighter chalcogenoyl homologue $SOCl_2$,[31] as well as the lighter selenoyl halide $SeOF_2$.[32] The Se–Cl bond lengths (216.5(1) pm – 220.0(1) pm) are significantly longer than for the reported $[SeCl_3]^+$ compounds, whereby the Se–O bond length (159.6(3) pm – 161.7(3) pm) is slightly shorter compared to $SeOF_2$. The compound shows an extensive formation of chalcogen bonds (ChB), leading to macromolecular arrangements, with Se···O distances between 275.6(3) pm and 298.0(3) pm, which is in good agreement to the above-mentioned homologues (see Figure 2).

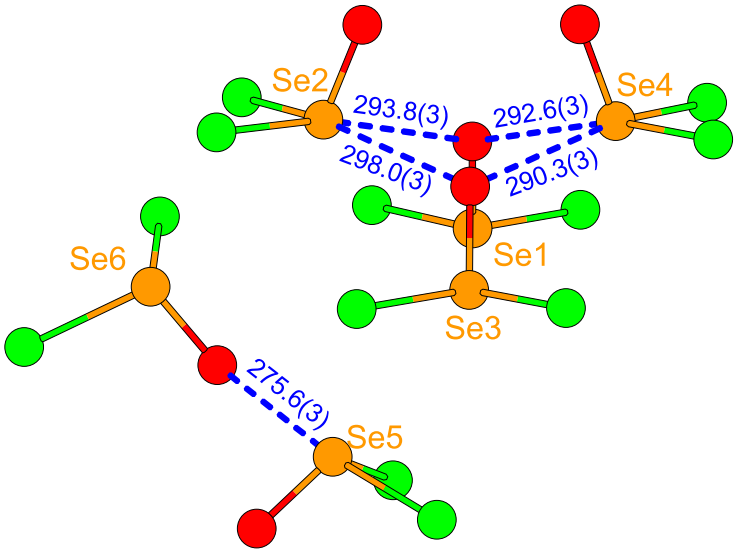

Figure 2: Assembly of the six crystallographically distinguishable $SeOCl_2$ units within the asymmetric unit of the crystal structure. Blue, dotted lines indicate chalcogen-bonding between the units, interatomic distances are given in [pm].

The Cl–Se–Cl angles (94.54(4)° – 96.61(6)°) and the O–Se–Cl angles (102.3(1)° – 104.1(1)°) are significantly closer toward the tetrahedral geometry, which would be expected for a Se(IV) compound with stereochemically active lone-pair, compared to $SeOF_2$, but less tetrahedral than $SOCl_2$. Intriguingly, although reported in 1922, the next heavier homologue $SeOBr_2$, being a solid (m.p. ~42°C), still lacks crystallographic elucidation.[33] The chloroselenite anion, as an example of a related substructure, shows the same symmetry as $SeOCl_2$ and has been investigated concerning its different donor-acceptor bonding abilities.[34]

After the successful synthesis of $SeOCl_2$, we subsequently used it as a reagent for the preparation of $[SeCl_3]^+$ containing species. First, we prepared $[SeCl_3]_2[S_2O_7]$ (**1**), using

View Article Online
DOI: 10.1039/D6DT01140C

elemental sulfur, $SeOCl_2$ and neat SO_3 for a direct solvothermal synthesis in closed glass ampoules . The compound can be isolated after heating to 80°C and crystallizes as colorless crystals in the centrosymmetric space group *C*2/*c* (No. 15) with 4 formula units per unit cell (see ESI, p. 9–12). The compound shows elongated Se–Cl bond lengths (212.17(7) pm – 213.51(3) pm) compared to the literature-known species (e.g. 209.6(2) pm in the $[AsF_6]^-$ salt,[16] and 210(1) for the $[SbCl_6]^-$ salt.[12] The structure shows strong non-covalent interactions (ChB) between the $[S_2O_7]^{2-}$ oxoanions and the *Lewis*-acidic $[SeCl_3]^+$ cation (see ESI, Fig. S3), as already observed by our group for the (inter-)halogen and (poly-)chalcogen polysulfates. A comparison of the S–O bond lengths can be found in Table 1.

Table 1: S–O bond lengths (in pm) and δ-values (terminal SO_3) groups of literature-known disulfate compounds. [DS] = $[S_2O_7]^{2-}$.

Bond	$[SeCl_3]_2[DS]$[a]	$[ReO_2Cl][DS]$[35]	$[ICl_2]_2[DS]$[20]	$Te[DS]_2$[36]b	$Bi[DS]_3$[37]b	$Li_2[DS]$[38]
S1–O11	144.14(9)	141.6(4)	143.6(4)	151.6	145.3	143.0(2)
S1–O12	143.27(8)	146.9(4)	141.1(3)	141.25	142.9	145.2(2)
S1–O13	144.27(9)	148.1(4)	142.5(4)	141.75	144.7	143.0(2)
S1–O121	163.54(6)	162.2(4)	163.3(3)	165.5	163.3	166.7(2)
δ(S1)	*13.21*	*13.38*	*13.09*	*12.51*	*13.33*	*12.11*
S2–O21		141.4(4)	145.0(3)	157.2	144.9	145.3(2)
S2–O22		142.5(4)	142.1(3)	141.3	143.2	145.1(2)
S2–O23		154.2(4)	145.2(3)	141.05	144.7	145.3(2)
S2–O121		162.2(4)	164.0(3)	158.85	162.1	161.0(1)
δ(S2)		*13.18*	*12.57*	*14.76*	*12.36*	*13.31*

a – symmetry plane through the anion leads to S1 = S2. b–= the averaged values were used.

The $[S_2O_7]^{2-}$ anion shows slightly elongated terminal S–O bond lengths, which are in accordance with the observed strong cation-anion interactions found within compounds with highly charged (Te^{4+}) or strongly electrophilic (ICl_2^+) cations. The longer the terminal S–O bond, the shorter becomes the interatomic O···Se distance and the longer the opposite Se–Cl bond due to electron density donation into the antibonding σ^* orbital. The strong cation-anion interaction leads to pyramidalization of the terminal SO_3 unit, which is depicted in the increased *δ*-value (calculations details are given in the SI, Section C and were reported by our group before).[20, 39] If, in addition to comparison of the bond lengths, the macromolecular assembly of the $[SeCl_3]_2[S_2O_7]$ ion pairs is considered, the resulting macrocycle shows a strong resemblance to the molecular compound $ReO_2Cl[S_2O_7]$ (see Figure 3).[35] Although the Se···O distances are slightly above the sum of the van-der-Waals radii,[40] the adaption of the conformation found in the molecular disulfate indicates that the interactions are nearly covalent.

View Article Online
DOI: 10.1039/D6DT01140C

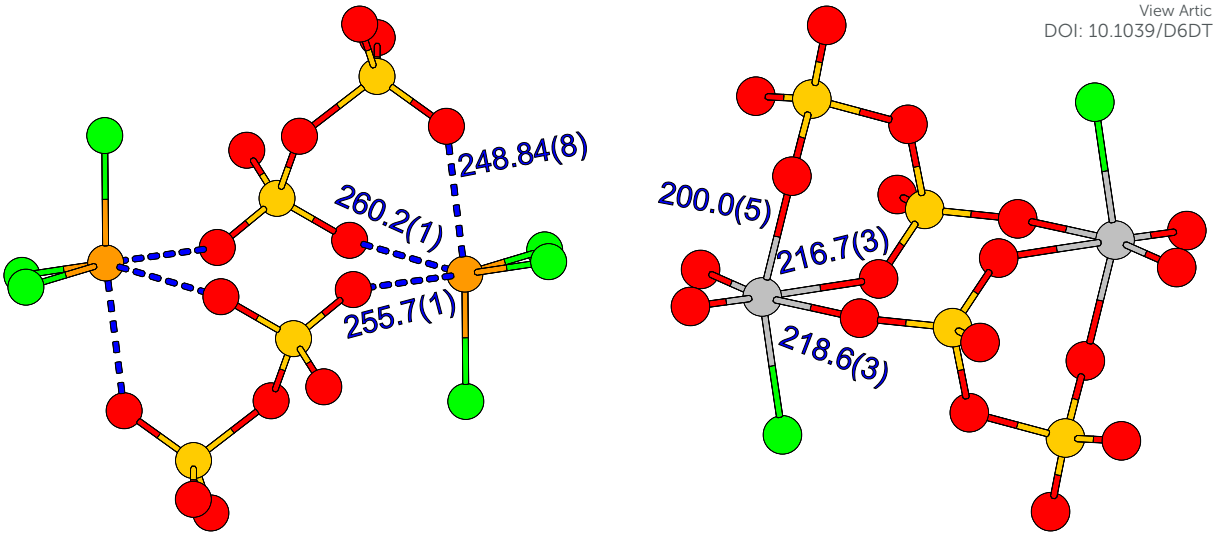

Figure 3: Dimeric macrocycle formed via chalcogen bonding in $[SeCl_3]_2[S_2O_7]$ (left) and literature-known molecular entity $[ReO_2Cl][S_2O_7]$[35] (right). Se/Re···O distances are given in [pm] (blue colored).

This further underlines the strength of the observed non-covalent interactions. The herein shown rings strongly differ in their conformation from classical organic systems, since the ring-building atoms cannot be classically described in their geometry by Csp^3 models, which makes conformational analysis challenging.[41]

If the reaction mixture $S_8 + SeOCl_3 + SO_3$ is not heated but stored at room temperature, colorless crystals grow at the interface of the originally obtained slurry and could be identified as $[SeCl_3][ClSO_3]$, which crystallizes in the triclinic space group $P\bar{1}$ (No. 2) with 8 formula units per unit cell. Similar to the observation for the starting material $SeOCl_2$, the large asymmetric unit (as well as the increased amount of crystallographically distinguishable building blocks) can be attributed to strong cation-anion interactions. This is not only evident in the increased Se–Cl bond lengths (212.5(2) pm – 214.7(1) pm), but also the elongated terminal S–O bond lengths of the $[ClSO_3]^-$ anion (see Table 2), which are comparable to the strong hydrogen-bond donor $[NH_4]^+$ and the strongly electrophilic $[NO]^+$.

Table 2**:** S–O and S–Cl bond lengths (in pm) of literature-known chlorosulfate compounds.

Bond	$[SeCl_3][ClSO_3]$[a]	$[NH_4][ClSO_3]$[42]	$Ca[ClSO_3]_2$[43]	$[NO][ClSO_3]$[44]
S–O11	143.85	144.70(9)	142.5	143.0
S–O12	143.98	143.26(9)	144.5	141.7
S–O13	144.65	144.50(9)	141.0	144.3
S–Cl	205.51	206.81(4)	200.4	205.3

a – the averaged values were used.

Although only few crystal structures of chlorosulfates were reported in the literature so far, the strongly increased S–O bond length compared to hard mono- and divalent cations like $[NO]^+$ and Ca^{2+} further suggests that the $[SeCl_3]^+$ cation is not only a strong *Lewis* acid but also shows that strong non-covalent interactions between the $[ClSO_3]^-$ anion and the cation are present. As

View Article Online
DOI: 10.1039/D6DT01140C

for the disulfate (**1**), this results in the formation of macromolecular cycles built of (**2**), as shown in Figure 4.

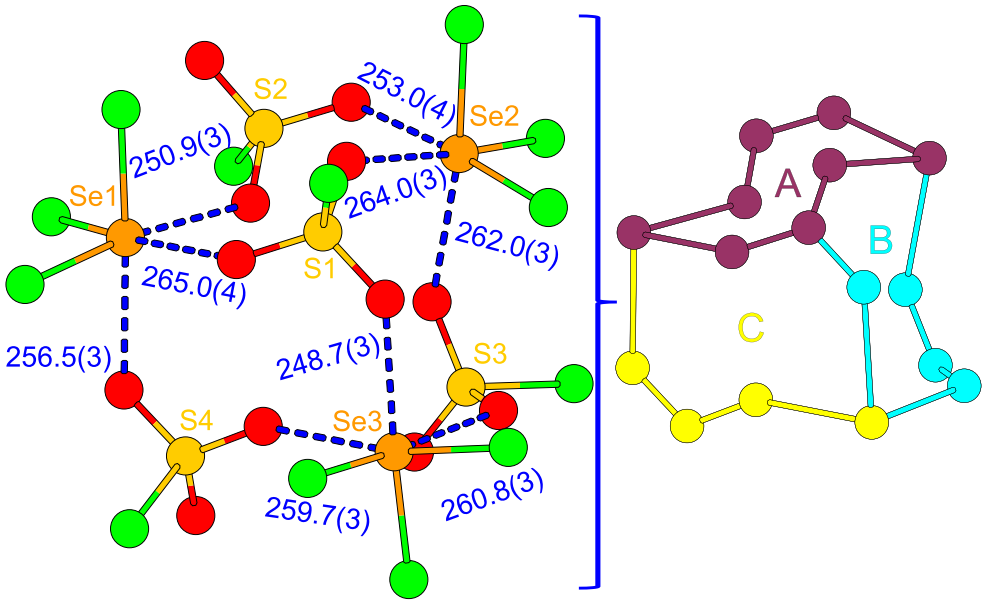

Figure 4: Chalcogen-bonding (D–A distance below 300 pm) within $[SeCl_3][ClSO_3]$ (left) and reduced representation of the formed macromolecular eight-membered rings (right). Distances are given in pm.

The resulting 'trimer' can be modelled as three condensed eight-membered rings, whereby each selenium atom is coordinated by three adjacent anions, leading to a distorted octahedral coordination. As for compound **1**, the interatomic O···Se distances are very short and correlate with elongated S–O and Se–Cl bond lengths of the respective *Lewis* basic donor and the *Lewis* acidic acceptor units. Notably, the observed bond lengths and interatomic distances for **1** and **2** are in a very narrow range, which means that the *Lewis* basicity of $[ClSO_3]^-$ and $[S_2O_7]^{2-}$ should be nearly the same. This is surprising, since the respective (gas phase) acidities of the parent acids are still significantly different.[45-46]

The phase pure preparation of compounds **1** and **2** has yet to be achieved, although we were able to identify both phases several times on the diffractometer. Due to the stark oxidative strength of neat SO_3, the formation of bright yellow and orange-colored solutions and solids can be observed, especially upon heating, which indicate the formation of $[Se_4]^{2+}$ cations.[47] Additionally, the compounds are still highly reactive towards moisture or other nucleophilic reagents, which is why no additional analyses (i.e. vibrational spectroscopy or thermal stability studies) were conducted so far.

In addition to compounds **1** and **2**, we sought to isolate reference di-/chlorosulfates with the $[SeBr_3]^+$ or $[SeI_3]^+$ cation. We were not able to receive any $[SeBr_3]^+$ compound when reacting the elements with neat SO_3, but observed the formation of $[Se_4][S_4O_{13}]$.[48] When elemental selenium and iodine are reacted with neat SO_3 at 80°C, dark-blue/purple crystals can be isolated from the green/blue mother liquor. The respective crystals were shown to be the compound $[Se_2I_4][S_4O_{13}](SO_3)$ (**3**), which crystallizes in the triclinic space group $P\bar{1}$ (No. 2), whereby the free SO_3 unit is slightly disordered (see Figure 5).

View Article Online
DOI: 10.1039/D6DT01140C

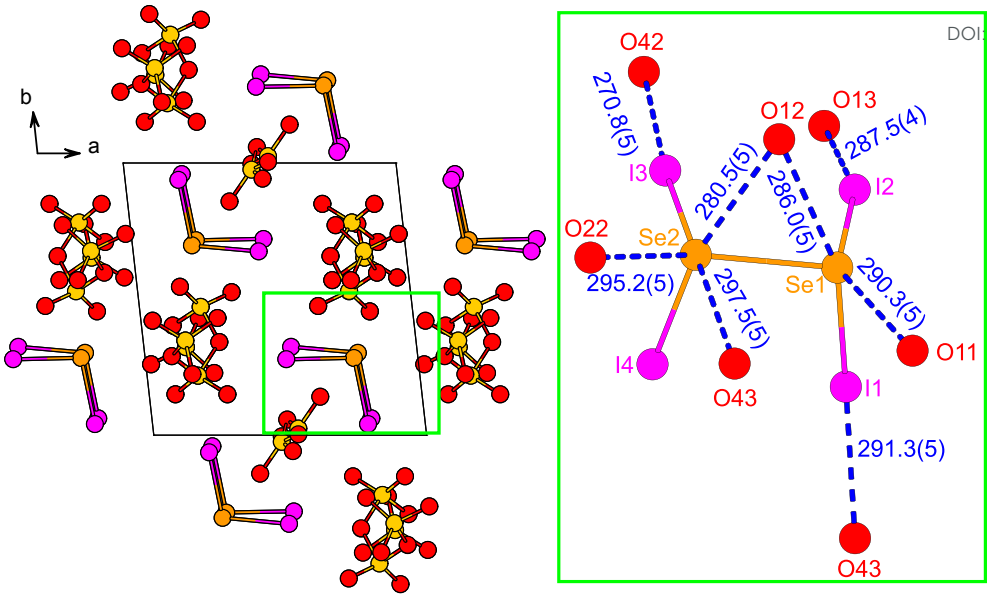

Figure 5: Extended unit cell of $[Se_2I_4]_2[S_4O_{13}]_2 \cdot (SO_3)$, viewed along the crystallographic c-axis (left) and chalcogen-bonding and halogen-bonding (D–A distances below 300 pm) within $[Se_2I_4]_2[S_4O_{13}]_2 \cdot (SO_3)$ (right). Distances are given in pm.

The cation was already reported as an $[AsF_6]^-$ and an $[Sb_2F_{11}]^-$ salt,[49] yet the compound is another addition to the group of the still scarcely found tetrasulfates. Unlike for the fluoropnictogenates, which were able to stabilize $[SeI_3]^+$ as an $[AsF_6]^-$ salt as well, we were so far not able to achieve this.[50] However, since a variety of mixed Se/I cations were already isolated or proposed to exist in equilibria within solutions,[51] the isolation of an $[SeI_3]^+$ (poly-)sulfate compound should be possible by adjusting the reaction system. The novel tetrasulfate **3** shows significantly shortened Se–Se bond lengths (271.9(1) pm) and elongated Se–I bond lengths (247.56(8) pm – 248.46(8) pm) compared to the literature-known fluoropnictogenate (Se–Se: 284.1(2) / 284.0(6) and Se–I: 243.6(2)–245.7(2) / 244.6(4)–246.0(4) pm for the $[Sb_2F_{11}]^-$ / $[AsF_6]^-$ salt). As for the fluoropnictogenates, the cation adopts a *cis*-like conformation, similar to P_2I_4.[52]

The short Se–Se bond is more comparable to the neutral $[N_4Se_4]$.[53] While the elongated Se–I bonds already indicate a certain degree of HaB between the oxoanion and the sigma-holes at the iodine atoms, the starkly shortened Se–Se bond suggests that the theoretically possible dissociation of $[Se_2I_4]^{2+}$ into $2[SeI_2]^{\cdot+}$ would be strongly disfavored in an oxoanionic environment. In other words, the proposed π^*–π^* interaction of the SOMO's of two $[SeI_2]^{\cdot+}$ cations would be favored in an oxoanionic environment. This matches the observations we already made for the $[I_4]^{2+}$ cation and shows that polysulfates might be particular attractive for the stabilization of homoconjugated polycations.[54]

If the S–O bond lengths within compound **3** (see ESI, Table S 24) are compared to some of the literature-known tetrasulfates, the influence of non-covalent interactions gets more visible. In contrast to compound **1** and **2**, although the selenium atoms formally bear a positive charge, they are not the strongest *Lewis* acidic centers in terms of coordination (see ESI, Fig. S 9), but strong HaB between the terminal oxygen atoms and the σ-holes of the iodine atoms are observed. The terminal and bridging S–O bond lengths are in good agreement to compounds

View Article Online
DOI: 10.1039/D6DT01140C

like $[I_3]_4[S_4O_{13}]_2(SO_3)$ and $[Te_6][S_4O_{13}]_2$.[20-21], confirming the stronger cation-anion interaction compared to classical group I/II polysulfates like $Li_2[S_4O_{13}]$ or $Ba[S_4O_{13}]$.[37]

Quantum Chemical Calculations

To complement the experimental X-ray diffraction data, Density Functional Theory (DFT) calculations were performed to analyze the supramolecular assemblies of compounds **1**–**3** and the starting reagent $SeOCl_2$. The theoretical study focused on characterizing the strength and directionality of the concurrent halogen- and chalcogen bonds governing the crystal packing. Molecular Electrostatic Potential surfaces were calculated for the $SeOCl_2$ monomer, the cationic units of the salts, and the co-crystallized SO_3 moiety to visualize the σ-hole and π-hole donor capabilities. To quantify and classify the non-covalent interactions, the topological analysis of the electron density was conducted using the Quantum Theory of Atoms in Molecules[55] in conjunction with the Non-Covalent Interaction (NCIplot) index.[56] Due to the significant ionic character of the solid-state structures, the binding energies of the specific ChB and HaB contacts were estimated using energy predictors based on the potential energy density ($V(r)$) at the bond critical points. Furthermore, Natural Bond Orbital analysis was employed to investigate charge transfer effects and to rationalize the interactions from an orbital donor-acceptor perspective.

The MEP surface of $SeOCl_2$ (c.f. Figure 6) reveals the presence of three σ-holes on the Se atom, located opposite to the Se–Cl and Se–O bonds. The electrostatic potentials at these regions are very similar, with values of 35.6 kcal/mol (opposite Se–Cl) and 33.5 kcal/mol (opposite Se–O), anticipating a comparable ability of the three σ-holes to interact with electron-rich domains. The MEP minimum is located at the O-atom (–25.8 kcal/mol), while the σ-hole on the Cl-atom is significantly less positive (12.5 kcal/mol), which explains the absence of HaB interactions in the crystal lattice. A partial view of the experimental X-ray structure confirms that the three σ-holes at the Se-atom participate in ChB interactions, forming three Se···O contacts with similar distances, in excellent agreement with the MEP analysis. To further characterize these interactions, QTAIM and NCIplot analyses were performed on two representative dimers (Figure 6c,d). In both cases, the ChB is characterized by a bond critical point (BCP, red sphere) and a bond path (orange line) connecting the Se and O atoms. Additionally, disk-shaped RDG isosurfaces, colored in green to indicate weak interactions, appear coincident with the location of the BCPs. The computed interaction energies derived from the QTAIM data are –2.1 kcal/mol for the ChB opposite the Se–Cl bond and –2.3 kcal/mol for the ChB opposite the Se–O bond. This slightly higher stability agrees well with the shorter interatomic distance observed in the solid state for the contact opposite to the Se–O bond.

View Article Online
DOI: 10.1039/D6DT01140C

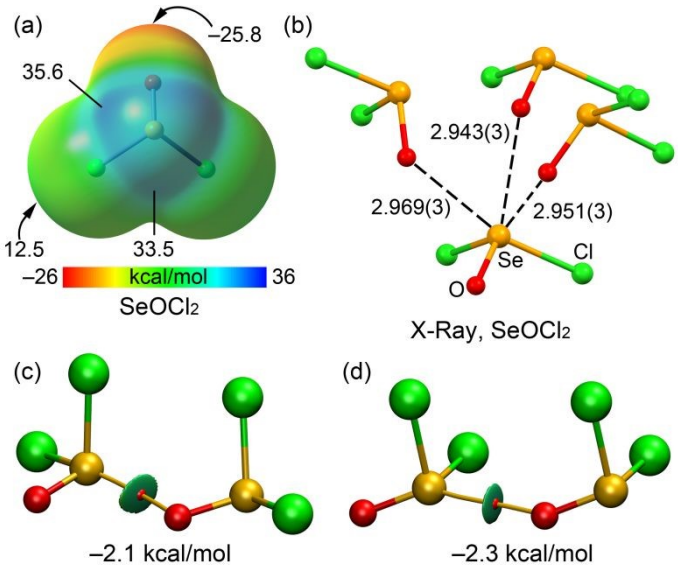

Figure 6: (a) Molecular Electrostatic Potential surface of the $SeOCl_2$ monomer (isosurface 0.001 a.u.) with energies at selected points in kcal/mol. (b) Partial view of the X-ray structure of $SeOCl_2$ showing the ChB interactions and distances in Å. (c,d) QTAIM/NCIplot analysis of two representative $SeOCl_2$ dimers showing the BCPs (red spheres), bond paths (orange lines) and RDG isosurfaces (green disks) characterizing the Se···O chalcogen bonds. The interaction energies in kcal/mol are also indicated.

The MEP surface of the $[SeCl_3]^+$ cation (see ESI, Fig. S 7) shows, as expected for a cationic species, a positive electrostatic potential over the entire surface. The surface presents three pronounced maxima corresponding to the σ-holes on the Se atom, located opposite to the Se–Cl bonds, with a value of 151 kcal/mol. In contrast, the potential at the σ-hole of the chlorine atom is significantly less positive (114 kcal/mol), while the minimum value on the surface is found at the electronic belt of the chlorine atoms (96.6 kcal/mol). This directly impacts the crystal packing, leading to establishment of supramolecular cycles through bifurcated Se···O,O contacts. These assemblies demonstrate that, despite the dominant nondirectional coulombic forces, the directionality of the σ-hole interactions plays a crucial role in fine-tuning the final solid-state architecture.

QTAIM and NCIplot analyses for salts **1** and **2** are shown in Figure 7. Within compound **1**, a bidentate Se···O,O dimer is present, where each chalcogen bond is characterized by a BCP and a bond path connecting the selenium and oxygen atoms. A dark blue RDG isosurface is observed between the interacting atoms, revealing the strong nature of these contacts, corroborated by the computed interaction energies of –5.1 and –6.7 kcal/mol, which are more than double the values obtained for the neutral $SeOCl_2$ monomer. A similar energetic landscape is found for the monodentate interaction between the $[S_2O_7]^{2-}$ anion and two $[SeCl_3]^+$ cations, where the strength of each Se···O contact is estimated at –5.4 kcal/mol. In contrast, the Cl···O halogen bond observed in compound is characterized by a small, much weaker interaction, with a computed strength of –1.4 kcal/mol.

The analysis of a representative ChB in compound **2** (Figure 7d) reveals topological features similar to those in compound **1** (BCP, bond path, and dark blue RDG isosurface), with an interaction energy of –6.6 kcal/mol.

View Article Online
DOI: 10.1039/D6DT01140C

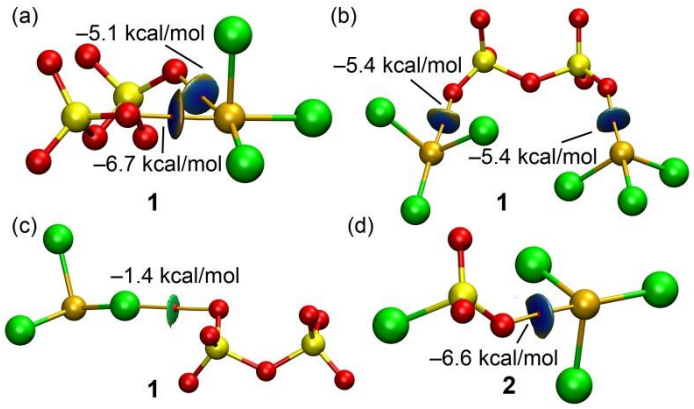

Figure 7: QTAIM distribution of bond critical points (red spheres) and bond paths (orange lines) and NCIplot isosurfaces for selected dimers of compound **1** (a-c) and **2** (d). The interaction energies in kcal/mol are also indicated.

An NBO analysis was performed to evaluate the orbital contributions to the stability of the assemblies in compounds **1** and **2** (see ESI, Fig. S 8). The chalcogen bonding interactions in both compounds are characterized by a substantial electron donation from the lone pair (LP) orbital of the anionic oxygen atom to the antibonding σ^* (Se–Cl) orbital of the cation. This confirms the LP→σ* charge transfer nature of these contacts, which is typical for σ-hole interactions. The second-order perturbation energies $E^{(2)}$ associated with these donors-acceptor interactions are quite large, ranging from 20.4 to 30.1 kcal/mol.

The MEP surface of the SO_3 molecule (see ESI, Fig. S 9) exhibits two π-holes located above and below the central S-atom, corresponding to the MEP maxima (56.1 kcal/mol). The minima are found at the three oxygen atoms with quite modest values (-11.5 kcal/mol), indicating very low nucleophilicity. The SO_3 monomer participates in two concurrent π-hole interactions in the solid-state structure of **3**, acting as a Lewis acid toward the oxygen atoms of two $[S_4O_{13}]^{2-}$ anions with distances of 274.5(8) pm and 299.3(8) pm. Each S···O π-hole interaction is characterized by a BCP, a bond path, and a green RDG isosurface, showing weak computed interaction strengths of –1.7 kcal/mol for the longer contact and –3.7 kcal/mol for the shorter one (see ESI, Fig. S 10). This is in good agreement to our reported values for the SO_3 coordination within $[I_3]_4[S_4O_{13}]_2(SO_3)$.[20]

The MEP surface of the $[Se_2I_4]^{2+}$ dication is significantly more complex (see ESI, Fig. S 9). On one side, two deep σ-holes (213 kcal/mol) are observed on the selenium atoms, formed as a consequence of the merging of the two σ-holes opposite to the Se–I bonds. The MEP minimum is located at the electronic belt of the iodine atoms (151 kcal/mol). The iodine atoms also present significantly positive σ-holes (191 kcal/mol), suggesting that a degree of competition between ChB and HaB is to be expected in this system. The color of the RDG isosurfaces reveals a clear distinction between the contacts: a strong, directional I···O interaction (blue isosurface) and a weak, secondary I···O contact (green isosurface), corroborated by the calculated interaction energies of –8.6 kcal/mol and –1.0 kcal/mol, respectively. A partial view of the X-ray structure of **3** shows that one oxygen atom of the anion is positioned precisely at the location predicted by the MEP where the merged σ-hole is present, forming a bifurcated (bidentate) Se,Se···O ChB. Each individual Se···O contact is significantly weaker (-3.1 and -2.7 kcal/mol) than the primary I···O halogen bond. However, the collective strength of this

View Article Online
DOI: 10.1039/D6DT01140C

bifurcated ChB motif is –5.8 kcal/mol, which is comparable to the ChB strengths found in compounds **1** and **2**.

Concurrently, another oxygen atom interacts in a monodentate fashion with the iodine atom of a neighboring cation. In stark contrast to compound **1** (where the lighter Cl atom was involved), the HaB and ChB distances in compound **3** are very similar (ranging from 280.5(5) pm to 287.5(4) pm), confirming the strong competition between both types of interactions. When strong electrostatic effects are excluded (as in these QTAIM-based estimations), the halogen bond in compound **3** is intrinsically stronger than the chalcogen bond. This trend agrees well with the higher polarizability and superior σ-hole donor ability of the iodine atom compared to the selenium atom.

To complete the theoretical characterization of compound **3**, an NBO analysis was performed to visualize the orbital donor-acceptor interactions (c.f. Figure 8). In the π-hole assembly, a clear LP(O)→π*(S=O) electron of the anionic oxygen atoms is observed, confirming the π-hole nature of the SO_3 coordination, while the computed second-order perturbation energies $E^{(2)}$ are relatively modest (1.0 and 3.7 kcal/mol), which is in line with the long S···O intermolecular distances described previously. The halogen-bonded dimer presents the expected LP(O)→σ*(Se–I) charge transfer. In this case, the $E^{(2)}$ energy is very large (25.7 kcal/mol), revealing a strong orbital overlap consistent with the directional nature of the HaB. Finally, for the bifurcated Se,Se···O ChB, the same oxygen lone pair donates electron density simultaneously into two σ*(Se–I) orbitals. This corroborates the bifurcated nature of the interaction and explains the smaller individual $E^{(2)}$ values (8.1 and 9.7 kcal/mol), as the electron transfer is shared by a single donor orbital. However, the combined stabilization energy of 17.8 kcal/mol remains substantial, highlighting the importance of these cooperative orbital effects in the crystal packing.

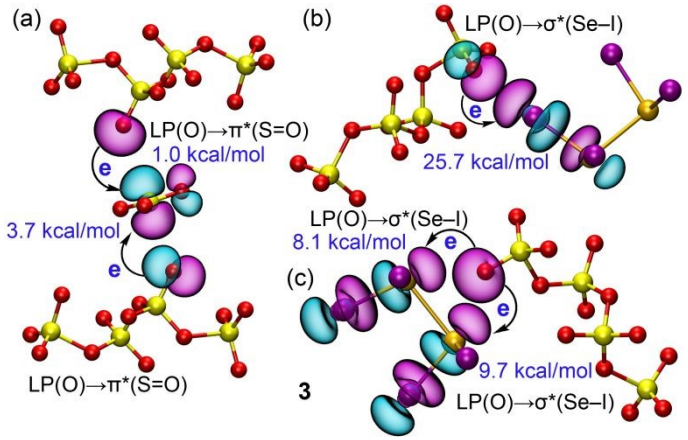

Figure 8: NBO analysis of the non-covalent assemblies in compound **3**. (a) LP(O)→π*(S=O) interactions in the π-hole assembly. (b) LP(O)→σ*(Se–I) interaction in the halogen-bonded dimer. (c) Dual LP(O)→σ*(Se–I) interactions in the bifurcated chalcogen-bonded dimer. The associated second-order perturbation energies $E^{(2)}$ in kcal/mol are indicated.

Conclusions

The theoretical study of $SeOCl_2$ confirmed that chalcogen bonding dominates the self-assembly of the neutral building block, driven by the three σ-holes on the selenium atom, while halogen bonding is absent due to the poor electrophilicity of the chlorine atoms. Upon moving to the cationic species in salts **1** and **2**, the depth of the selenium σ-holes increases dramatically,

View Article Online
DOI: 10.1039/D6DT01140C

leading to strong, electrostatically reinforced Se···O chalcogen bonds that define the solid-state architecture, with Cl···O halogen bonds playing only a secondary role.

In contrast, the introduction of iodine in salt **3** fundamentally alters the interaction landscape. The $[Se_2I_4]^{2+}$ cation exhibits a distinct competition between iodine-based halogen bonds and selenium-based chalcogen bonds. The I···O halogen bonds are intrinsically stronger and more directional than the bifurcated Se···O interactions, a trend consistent with the higher polarizability and superior σ-hole donor ability of iodine. These novel insights highlight that the border between strong non-covalent interactions and covalency can be slowly approached within oxoanionic media. As already proposed by *Gillespie* for the reaction between SeF_4 and SO_3 in FSO_3H solutions, the formation of 'adducts',[57] which could not be described as ionic anymore, seems to be at the end of this range.

Author contributions

M. S. W. and J. L. planned and designed the project. J. L. synthesized and characterized the compounds. A. F. and S. B. planned and conducted the theoretical studies. J.L. wrote the first draft of the manuscript. All authors participated in preparing the final draft of the manuscript.

Conflict of Interest

The authors declare no conflict of interest.

Acknowledgements

J.L. is thankful to the German National Scholarship Foundation (Studienstiftung) for financial support.

Keywords:

Chalcogen-bonding, Polysulfates, Density functional theory, Solid-state structures, Sulfur Trioxide

TOC Graphic:

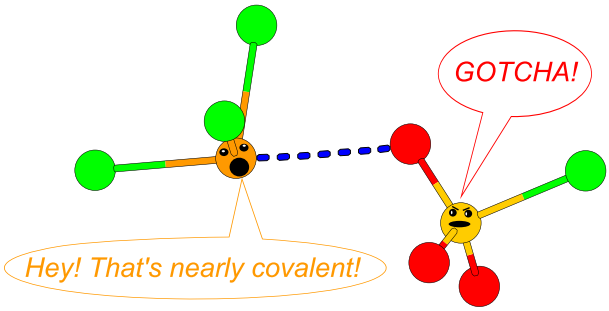

Caption: Within the novel, oxoanionic $[SeCl_3]$ salts, e.g. $[SeCl_3][ClSO_3]$, the observed non-covalent interactions and the macromolecular assemblies formed due to them are already comparable to the interactions known from molecular (i.e. covalent) compounds!

View Article Online
DOI: 10.1039/D6DT01140C

Uncategorized References

[1] F. Clausnizer, *Liebigs Ann.* **1879**, *196*, 265-298.
[2] A. Stähler, B. Tesch, *Z. Anorg. Allg. Chem.* **1916**, *98*, 1-26.
[3] B. Krebs, F.-P. Ahlers, *Adv. Inorg. Chem.* **1990**, *35*, 235-317.
[4] A. W. Cordes, R. F. Kruh, E. K. Gordon, M. K. Kemp, *Acta Crystallographica* **1964**, *17*, 756.
[5] P. Born, R. Kniep, D. Mootz, *Z. Naturforsch. B* **1981**, *36*, 1516-1519.
[6] R. Kniep, L. Körte, D. Mootz, *Z. Naturforsch. B* **1981**, *36*, 1660-1662.
[7] L. Kolditz, W. Schäfer, *Z. Anorg. Allg. Chem.* **1962**, *315*, 35-45.
[8] H. Gerding, *Recl. Trav. Chim. Pays-Bas* **1956**, *75*, 589-593.
[9] E. A. Robinson, J. A. Ciruna, *Can. J. Chem.* **1968**, *46*, 3197-3200.
[10] H. Gerding, D. Stufkens, H. Gijben, *Recl. Trav. Chim. Pays-Bas* **1970**, *89*, 619-624.
[11] R. Kapoor, P. Wadhawan, V. Katyal, V. R. Sood, P. Kapoor, *Can. J. Chem.* **1989**, *67*, 1760-1764.
[12] B. H. Christian, M. J. Collins, R. J. Gillespie, J. F. Sawyer, *Inorg. Chem.* **1986**, *25*, 777-788.
[13] B. Neumüller, C. Lau, K. Dehnicke, *Z. Anorg. Allg. Chem.* **1996**, *622*, 1847-1853.
[14] J. Beck, P. Biedenkopf, K. Müller-Buschbaum, J. Richter, K.-J. Schlitt, *Z. Anorg. Allg. Chem.* **1996**, *622*, 292-296.
[15] A. Baumann, J. Beck, *Z. Anorg. Allg. Chem.* **1998**, *624*, 1725-1726.
[16] J. Passmore, P. D. Boyle, G. Schatte, T. Way, T. S. Cameron, *Can. J. Chem.* **1996**, *74*, 1671-1681.
[17] J. M. Rautiainen, T. Way, G. Schatte, J. Passmore, R. S. Laitinen, R. J. Suontamo, J. Valkonen, *Inorg. Chem.* **2005**, *44*, 1904-1913.
[18] T. M. Klapötke, C. M. Rienäcker, *Z. Anorg. Allg. Chem.* **1994**, *620*, 2104-2107.
[19] M. A. Bonnin, L. Bayarjargal, V. Milman, B. Winkler, C. Feldmann, *Inorg. Chem. Front.* **2023**, *10*, 2636-2644.
[20] J. Langwald, R. M. Gomila, D. van Gerven, A. Frontera, M. S. Wickleder, *Dalton Trans.* **2025**, *54*, 16095-16105.
[21] J. Langwald, S. Burguera, A. Frontera, M. S. Wickleder, *Dalton Trans.* **2026**, *in press*.
[22] G. R. Desiraju, P. S. Ho, L. Kloo, A. C. Legon, R. Marquardt, P. Metrangolo, P. Politzer, G. Resnati, K. Rissanen, *Pure Appl. Chem.* **2013**, *85*, 1711-1713.
[23] L. Vogel, P. Wonner, S. M. Huber, *Angew. Chem. Int. Ed.* **2019**, *58*, 1880-1891.
[24] A. Frontera, A. Bauza, in *International Journal of Molecular Sciences, Vol. 22*, **2021**, p. 12550.
[25] R. Hein, P. D. Beer, *Chem. Sci.* **2022**, *13*, 7098-7125.
[26] M. Bujak, H.-G. Stammler, N. W. Mitzel, *Chem. Eur. J.* **2025**, *31*, e202404648.
[27] M. P. Hoffman, S. S. Xantheas, *J. Am. Chem. Soc.* **2025**, *147*, 11152-11171.
[28] I. Lindqvist, G. Nahringbauer, *Acta Crystallographica* **1959**, *12*, 638-642.
[29] G. Brauer, *Handbuch der Präparativen Anorganischen Chemie*, 3 ed., Ferdinand Enke Verlag, Stuttgart, **1975**.
[30] T. Kottke, D. Stalke, *J. Appl. Crystallogr.* **1993**, *26*, 615-619.
[31] D. Mootz, A. Merschenz-Quack, *Acta Crystallogr. C* **1988**, *44*, 926-927.
[32] J. C. Dewan, A. J. Edwards, *J. Chem. Soc., Dalton Trans.* **1976**, 2433-2435.
[33] V. Lenher, *J. Am. Chem. Soc.* **1922**, *44*, 1668-1673.
[34] R. T. Boeré, *Molecules* **2023**, *28*, 7489.
[35] U. Betke, W. Dononelli, T. Klüner, M. S. Wickleder, *Angew. Chem. Int. Ed.* **2011**, *50*, 12361.
[36] C. Logemann, J. Bruns, L. V. Schindler, V. Zimmermann, M. S. Wickleder, *Z. Anorg. Allg. Chem.* **2015**, *641*, 831-837.
[37] J. Bruns, C. Kolb, M. S. Wickleder, *Z. Anorg. Allg. Chem.* **2014**, *640*, 2345.
[38] C. Logemann, J. Witt, M. S. Wickleder, *Z. Kristallogr. NCS* **2013**, *228*, 159-160.
[39] L. Link, R. Niewa, *J. Appl. Crystallogr.* **2023**, *56*, 1855-1864.
[40] A. Bondi, *J. Phys. Chem.* **1964**, *68*, 441-451.
[41] J. Perez, K. Nolsoe, M. Kessler, L. Garcia, E. Perez, J. L. Serrano, *Acta Crystallographica Section B* **2005**, *61*, 585-594.
[42] V. Zimmermann, L. V. Schindler, D. van Gerven, M. S. Wickleder, *Z. Anorg. Allg. Chem.* **2022**, *648*, e202200238.

View Article Online
DOI: 10.1039/D6DT01140C

[43] S. Trojanov, V. Rybakov, E. Kemnitz, D. Hass, H. Worzala, *Z. Anorg. Allg. Chem.* **1990**, *585*, 204-208.
[44] T. Höhle, F. Mijlhoff, *Recl. Trav. Chim. Pays-Bas* **1967**, *86*, 1153-1158.
[45] I. A. Koppel, P. Burk, I. Koppel, I. Leito, T. Sonoda, M. Mishima, *J. Am. Chem. Soc.* **2000**, *122*, 5114-5124.
[46] A. H. Otto, R. Steudel, *Eur. J. Inorg. Chem.* **2001**, *2001*, 3047-3054.
[47] J. Langwald, S. Burguera Piña, A. Frontera, M. S. Wickleder, *Dalton Trans.* **2026**.
[48] E. Turgunbajew, M. Symeonidis, J. Langwald, L. Schumacher, H. A. Höppe, R. Pöttgen, J. Bruns, M. S. Wickleder, **2026**, *Unpublished work*.
[49] W. S. Nandana, J. Passmore, P. S. White, C. M. Wong, *Inorg. Chem.* **1990**, *29*, 3529-3538.
[50] J. Passmore, P. Taylor, *J. Chem. Soc., Dalton Trans.* **1976**, 804-807.
[51] M. M. Carnell, F. Grein, M. Murchie, J. Passmore, C.-M. Wong, *J. Chem. Soc., Chem. Commun.* **1986**, 225-227.
[52] Y. C. Leung, J. Waser, *J. Phys. Chem.* **1956**, *60*, 539-543.
[53] H. Barnighausen, T. von Volkmann, J. Jander, *Acta Crystallographica* **1966**, *21*, 571-577.
[54] D. van Gerven, S. Sutorius, J. Bruns, M. S. Wickleder, *ChemistryOpen* **2022**, *11*, e202200122.
[55] E. R. Johnson, S. Keinan, P. Mori-Sánchez, J. Contreras-García, A. J. Cohen, W. Yang, *J. Am. Chem. Soc.* **2010**, *132*, 6498-6506.
[56] J. Contreras-García, E. R. Johnson, S. Keinan, R. Chaudret, J.-P. Piquemal, D. N. Beratan, W. Yang, *J. Chem. Theory Comput.* **2011**, *7*, 625-632.
[57] R. J. Gillespie, W. A. Whitla, *Can. J. Chem.* **1969**, *47*, 4153-4157.
[58] R. King, S. Sangokoya, *Inorg. Chem.* **1987**, *26*, 2727-2730.
[59] Bruker AXS, *APEX 5 v2023.9-2* **2023**, Madsion, Winconsin, USA.
[60] SmartLabStudioII, *Rigaku Corporation* **2014**, Version 4.4.295.290.
[61] L. Krause, R. Herbst-Irmer, G. M. Sheldrick, D. Stalke, *J. Appl. Crystallogr.* **2015**, *48*, 3-10.
[62] O. V. Dolomanov, L. J. Bourhis, R. J. Gildea, J. A. K. Howard, H. Puschmann, *J. Appl. Crystallogr.* **2009**, *42*, 339-341.
[63] G. Sheldrick, *Acta Crystallogr. C* **2015**, *71*, 3-8.
[64] G. Sheldrick, *Acta Crystallogr. A* **2015**, *71*, 3-8.
[65] Crystal Impact GbR, *Diamond 4.6.8* **2022**, Bonn, Germany.
[66] C. Logemann, T. Klüner, M. S. Wickleder, *Angew. Chem. Int. Ed.* **2012**, *51*, 4997-5000.
[67] S. G. Balasubramani, G. P. Chen, S. Coriani, M. Diedenhofen, M. S. Frank, Y. J. Franzke, F. Furche, R. Grotjahn, M. E. Harding, C. Hättig, A. Hellweg, B. Helmich-Paris, C. Holzer, U. Huniar, M. Kaupp, A. Marefat Khah, S. Karbalaei Khani, T. Müller, F. Mack, B. D. Nguyen, S. M. Parker, E. Perlt, D. Rappoport, K. Reiter, S. Roy, M. Rückert, G. Schmitz, M. Sierka, E. Tapavicza, D. P. Tew, C. van Wüllen, V. K. Voora, F. Weigend, A. Wodyński, J. M. Yu, *J. Chem. Phys.* **2020**, *152*.
[68] C. Adamo, V. Barone, *J. Chem. Phys.* **1999**, *110*, 6158-6170.
[69] S. Grimme, S. Ehrlich, L. Goerigk, *J. Comput. Chem.* **2011**, *32*, 1456-1465.
[70] F. Weigend, R. Ahlrichs, *Phys. Chem. Chem. Phys.* **2005**, *7*, 3297-3305.
[71] K. A. Peterson, D. Figgen, M. Dolg, H. Stoll, *J. Chem. Phys.* **2007**, *126*.
[72] A. Bauzá, A. Frontera, *ChemPhysChem* **2020**, *21*, 26-31.
[73] A. E. Reed, R. B. Weinstock, F. Weinhold, *J. Chem. Phys.* **1985**, *83*, 735-746.
[74] E. D. Glendening, C. R. Landis, F. Weinhold, *J. Comput. Chem.* **2019**, *40*, 2234-2241.

Additional references were cited in the supporting information.[58-74]

View Article Online
DOI: 10.1039/D6DT01140C

Data Availability

The data supporting this article have been included as part of the supplementary information (SI). Supplementary information: including experimental details, synthesis, computational details, crystallographic information, and additional characterization data. See DOI: https:// doi.org/.

CCDC 2516864 (for $SeOCl_2$), 2492705 (for $[SeCl_3]_2[S_2O_7]$), 2499372 (for $[SeCl_3][ClSO_3]$) and 2492707 (for $[Se_2I_4]_2[S_4O_{13}]_2(SO_3)$) contain the supplementary crystallographic data for this paper.